IEEE Access
Multidisciplinary ⋮ Rapid Review ⋮ Open Access Journal

Received 21 June 2024, accepted 9 July 2024, date of publication 12 July 2024, date of current version 23 July 2024.

Digital Object Identifier 10.1109/ACCESS.2024.3427367

RESEARCH ARTICLE

Design of Unmanned Helicopter Distributed Electric Tail Rotor Controller Based on Improved Active Disturbance Rejection Control

QING-XIN ZHANG[1], YUN-FENG JI[2], FENG WANG[3], LEI PEI[2], AND ZHENG-MING CHA[4]

[1]Key Laboratory of General Aviation, Shenyang Aerospace University, Shenyang 110136, China
[2]School of Artificial Intelligence, Shenyang Aerospace University, Shenyang 110136, China
[3]Liaoning General Aviation Academy, Shenyang 110136, China
[4]AVIC Changhe Aircraft Industry (Group) Corporation Ltd., Jingdezhen 333002, China

Corresponding authors: Yun-Feng Ji (jyf2588458@163.com) and Qing-Xin Zhang (zhy9712_sau@163.com)

ABSTRACT In response to the critical implications of single tail rotor failures in unmanned helicopters, this study proposes a distributed electric tail rotor yaw channel controller that employs Active Disturbance Rejection Control (ADRC) techniques. A dynamics model was created for an unmanned helicopter with a distributed electric tail rotor. This model was then employed to verify the yaw channel tracking performance of the helicopter through simulation. The verification process involved the use of a cascaded dual closed-loop active disturbance rejection control strategy. The ADRC framework was enhanced by developing an improved fal function to replace the conventional fal function. This addressed the challenges of excessive error gain and overshoot oscillation in the Extended State Observer (ESO). A test setup for the distributed electric tail rotor of an unmanned helicopter was devised and constructed for empirical testing purposes. This setup was used as a reference for the 700-class electric model helicopter. The findings of the simulation demonstrate that the control strategy for the unmanned helicopter's distributed electric tail rotor, enhanced by the refined cascaded ADRC method, achieves superior response speed and minimized overshoot during yaw channel tracking. Furthermore, it displays a degree of enhanced robustness and improved control proficiency in comparison to the conventional ADRC approach. The outcomes of the test stand validate the efficacy of this control strategy.

INDEX TERMS Active disturbance rejection control, cascaded control, distributed electric tail rotor, fal function, unmanned helicopter.

I. INTRODUCTION

Unmanned helicopters, renowned for their exceptional flexibility, rapid velocity, and capability for aerobatic maneuvers, are employed in a wide range of sectors, including agriculture, military support, fire rescue, cinematic production, and electrical inspections. Nevertheless, failure of the tail rotor invariably results in significant incidents. Consequently, researchers are investigating novel tail rotor technologies with the objective of enhancing the flight performance of unmanned helicopters.

In Reference [1], various configurations of distributed electrically driven anti-torque systems for light helicopters are assessed, with the tri-duct variable speed configuration being identified as offering optimal performance. This configuration is therefore deemed to have prospective utility in forthcoming electric tail rotor systems for light helicopters. Reference [2] indicates that Bell Helicopters has unveiled a prototype helicopter that employs a distributed anti-torque system, outfitted with four independently driven electric ducted tail rotors. This design demonstrates that a fixed-pitch, variable-speed distributed electric tail rotor configuration can achieve redundancy, thereby enhancing safety.

Moreover, the control of the tail rotor plays a pivotal role in the unmanned helicopter control system. The tail rotor serves

The associate editor coordinating the review of this manuscript and approving it for publication was Binit Lukose.

two primary functions: to control the unmanned helicopter's yaw channel and to counteract the reactive torque generated by the main rotor. Consequently, the tail rotor system is also known as the anti-torque system. The manner in which the control method is employed has a direct impact on the flight dynamics of the unmanned helicopter. Currently, a plethora of techniques are available for the control of unmanned helicopter attitude.

Reference [3] employs a sequential quadratic programming algorithm to transform the nonlinear yaw model of unmanned helicopters into a linear representation. The PID gains are then fine-tuned based on H ∞ criteria, thereby achieving precise tracking control of the yaw channel. Reference [4] presents an advanced trajectory control approach that employs an enhanced teaching-learning-based optimization (iTLBO) technique. This strategy refines the parameters of the PID controller by minimizing the yaw error, thereby demonstrating the method's viability for unmanned helicopter systems. Reference [5] devised a dual-loop control structure for helicopters to navigate external disturbances and uncertainties effectively. The inner loop ensures system stability, minimizes error, and enhances robustness against parameter uncertainties and disturbances. The outer loop ensures optimal trajectory tracking while preventing actuator saturation. Reference [6] developed an intelligent control system for helicopters based on an adaptive neural fuzzy inference system. This system enables the adjustment of pitch and yaw angles to achieve comprehensive control of altitude and angular velocity. In Reference [7], a comprehensive control method was introduced that utilizes an extended state observer for real-time estimation and compensation of system disturbances, combined with a proportional-integral controller to reduce steady-state errors caused by input signals. Furthermore, the method employs optimized control gains from a Linear Quadratic Gaussian controller to enhance the helicopter's control precision. Reference [8] proposed a pioneering control strategy for dynamically unknown nonlinear helicopter systems that does not rely on function approximation. Reference [9] developed a control strategy for helicopter systems with uncertain parameters based on adaptive inversion, which demonstrates high robustness in the face of uncertain parameters. Reference [10] developed an adaptive predictive feedback control method that is capable of precise angle tracking and compensating for known system delays, while also fully considering system uncertainties. Reference [11] employed control rules derived from a fuzzy logic system model to address uncertainties and disturbances in helicopter systems. The application of Lyapunov's theorem for the stability analysis of the closed-loop system serves to guide the adaptation of fuzzy system parameters.

As modern control theory continues to evolve, an increasing number of control methodologies have emerged. However, the PID control method remains the most prevalent in the domain of unmanned helicopter control. However, given the complexity, nonlinearity, and strong coupling of control elements in unmanned helicopters, traditional PID control frequently fails to achieve optimal control outcomes. After a comprehensive analysis and enhancement of the limitations of PID control, Jing-Qing Han, a researcher, formally introduced the concept of Active Disturbance Rejection Control (ADRC) in 1988. Reference [12] describes the advantages of ADRC over PID in terms of its two-degree-of-freedom structure, which provides better performance in terms of set-point tracking and disturbance rejection. How ADRC can be combined with data-driven modeling and machine learning algorithms to effectively manage the uncertainty inherent in smart power generation systems is discussed. By using machine learning to predict system disturbances and using ADRC to compensate for these disturbances in real time, the overall robustness and adaptability of the control system will be significantly enhanced. In Reference [13], the authors address the difficulties of tuning ADRC in power plants with significant time delays. They propose quantitative tuning rules for a delayed ADRC structure based on a typical first-order plus time delay model. The efficacy of this approach has been empirically validated. Currently, the technology known as Active Disturbance Rejection Control (ADRC) has undergone a process of progressive maturation, with its application spectrum expanding continuously. It is noteworthy that ADRC methods have been implemented within the flight control systems of unmanned helicopters.

This study develops a distributed electric tail rotor controller for unmanned helicopters that leverages ADRC, thereby ensuring precise control over the yaw channel. The study addresses the jitter issues in the extended state observer, attributed to the non-smooth fal function, by devising an improved fal function as a replacement. This replacement augments the state estimation accuracy of the Extended State Observer (ESO). The design of the main control board's hardware module and the subsequent software development culminate in the independent establishment of a distributed electric tail rotor test platform. The superiority of the improved ADRC method, as demonstrated by software simulations, is corroborated by test bench trials, which validate the effectiveness and feasibility of the control method.

II. FLIGHT DYNAMICS MODELING OF UNMANNED HELICOPTERS BASED ON DISTRIBUTED ELECTRIC TAIL ROTORS

A. KINEMATIC AND DYNAMIC MODELING OF UNMANNED HELICOPTERS

An unmanned helicopter represents a complex nonlinear system characterized by multiple inputs and outputs, significant coupling, and considerable uncertainty. Consequently, the formulation of precise kinematic and dynamic models constitutes the initial step in understanding its operation. It is only through the delineation of its mathematical model and the analysis of its physical characteristics that a more optimal control strategy can be devised.

The body coordinate system oxyz is affixed to the unmanned helicopter, with the origin o located at the

helicopter's center of gravity. The longitudinal axis, designated by the symbol "o," is situated within the helicopter's symmetrical plane and passes through the center of gravity. It is aligned with the longitudinal axis of the fuselage and oriented in a positive direction towards the nose. The vertical axis, oz, also passes through the center of gravity, parallel to the hub axis within the symmetrical plane of the fuselage, and directed positively downwards. The lateral axis oy, which passes through the center of gravity o, is perpendicular to the xoz plane and directed positively towards the left side of the fuselage. Figure 1 depicts an unmanned helicopter equipped with distributed electric tail rotors.

In this study, the unmanned helicopter is modeled as an ideal rigid body, with the assumption that the effects of elastic deformation are negligible. The dynamic equations are derived based on Newton's second law, expressed in vector form as follows [14].

$$\sum F = \frac{d}{dt}mV \tag{1}$$

In this context, F denotes the total external force exerted on the body, m signifies the mass of the unmanned helicopter, and V represents the velocity of the helicopter's center of mass.

In the body's coordinate system, the torque equilibrium equation for the unmanned helicopter is derived from the Newton-Euler equations, as illustrated in equation [15].

$$\sum M = I\dot{w}_b + (w_b \times Iw_b) \tag{2}$$

where I denotes the inertia tensor of the unmanned helicopter, ω_b denotes the body's angular velocity around the rotational axis, M signifies the total external torque exerted on the body.

By decomposing the total external force and torque relative to the body's coordinate system, the linear motion equations pertaining to the three principal axes are derived as follows:

$$\begin{cases} \sum F_x = m(-vr + wq + \dfrac{du}{dt}) \\ \sum F_y = m(-wp + ur + \dfrac{dv}{dt}) \\ \sum F_z = m(-uq + vp + \dfrac{dw}{dt}) \end{cases} \tag{3}$$

The quantities F_x, F_y, and F_z correspond to the sums of the total external force projections onto the O_x, O_y, and O_z axes, respectively. u, v, and w denote the linear velocities along these three axes. In addition, p, q, and r represent the angular velocities of the body about the x, y, and z axes, respectively. The governing equations for angular motion are articulated as follows:

$$\begin{cases} \sum M_x = (I_{zz} - I_{yy})qr - I_{xz}(\dfrac{dr}{dt} + pq) + I_{xx}\dfrac{dp}{dt} \\ \sum M_y = (I_{xx} - I_{zz})pr - I_{xz}(-r^2 + p^2) + I_{yy}\dfrac{dq}{dt} \\ \sum M_z = (I_{yy} - I_{xx})pq - I_{xz}(-qr + \dfrac{dp}{dt}) + I_{zz}\dfrac{dr}{dt} \end{cases} \tag{4}$$

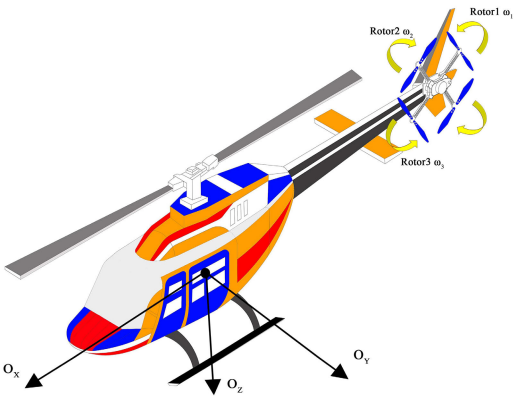

FIGURE 1. Illustration of an unmanned helicopter with distributed electric tail rotors.

The symbols M_x, M_y, and M_z correspond to the aggregated projections of the total external torque along the O_x, O_y, and O_z axes, respectively. I_{xx}, I_{yy}, and I_{zz} denote the moments of inertia of the unmanned helicopter about the O_x, O_y, and O_z axes, respectively. I_{xz} represents the product of inertia concerning the O_x and O_z axes. For the purposes of this study, the sign of torque is defined as positive when rotation occurs in the clockwise direction as viewed along the body axis. The equation delineating the body's attitude motion is presented below.

$$\begin{cases} \dfrac{d\varphi}{dt} = (q\sin\varphi + r\cos\varphi)\tan\theta + p \\ \dfrac{d\theta}{dt} = -r\sin\varphi + q\cos\varphi \\ \dfrac{d\psi}{dt} = \dfrac{q\sin\varphi + r\cos\varphi}{\cos\theta} \end{cases} \tag{5}$$

The symbols φ, θ, and ψ specifically denote the roll angle, pitch angle, and yaw angle of the helicopter, respectively. In summary, we derive the nonlinear dynamic equation for the unmanned helicopter as presented below.

$$\begin{bmatrix} \dot{u} \\ \dot{v} \\ \dot{w} \\ \dot{p} \\ \dot{q} \\ \dot{r} \\ \dot{\varphi} \\ \dot{\theta} \\ \dot{\psi} \end{bmatrix} = \begin{bmatrix} \sum \frac{F_x}{m} - wq + vr \\ \sum \frac{F_y}{m} + wp - ur \\ \sum \frac{F_z}{m} - vp + uq \\ \sum \frac{M_x}{I_{xx}} + \frac{I_{yy}-I_{zz}}{I_{xx}}qr \\ \sum \frac{M_y}{I_{yy}} + \frac{I_{zz}-I_{xx}}{I_{yy}}pr \\ \sum \frac{M_z}{I_{zz}} + \frac{I_{xx}-I_{yy}}{I_{zz}}pq \\ (q\sin\varphi + r\cos\varphi)\tan\theta + p \\ -r\sin\varphi + q\cos\varphi \\ \frac{q\sin\varphi + r\cos\varphi}{\cos\theta} \end{bmatrix} \tag{6}$$

Since the unmanned helicopter is almost symmetric about the left and right, that is, symmetric relative to the x-z

plane, it is approximated as zero. Consequently, the dynamic equation for the yaw rate in the body coordinate system can be obtained [16]:

$$\dot{r}I_{zz} = (I_{xx} - I_{yy})pq + N \tag{7}$$

where N denotes the torque acting on the body's z-axis.

B. DISTRIBUTED ELECTRIC TAIL ROTOR FORCE AND TORQUE MODEL

During hovering or cruising phases of the unmanned helicopter, where the pitch and roll velocities approach zero, the model can be simplified by setting $p = 0$ and $q = 0$. Consequently, this transformation modifies (7) to become (8):

$$\dot{r}I_{zz} = N \tag{8}$$

The torque exerted on the body's Z-axis is predominantly comprised of the N_m torque from the main rotor's rotation and the yaw-direction torque N_t,which arises from the total thrust T_t of the distributed electric tail rotor. The torque N acting on the body's Z-axis can be derived using Blade Element Theory or Momentum Theory, as illustrated in (9) [17]:

$$N = N_m + N_t \tag{9}$$

The torque N_m generated by the rotation of the main rotor is determined by the power P_m consumed by the rotation of the main rotor, expressed as:

$$N_m = -\frac{P_m}{\Omega_m} \tag{10}$$

The negative sign indicates that the direction of N_m is always opposite to the z-axis direction, driving the body in a counterclockwise direction. Ω_m represents the rotational speed of the main rotor, whereas P_m quantifies the total power expenditure during the main rotor's rotation. The total power consumption of the main rotor rotation encompasses the profile power consumption P_{pro}, induced power consumption P_{ind}, parasitic power consumption P_{par}, and climbing power consumption P_{cli}, respectively represented as follows:

$$\begin{cases} P_{pro} = (\Omega_m^2 R_m^2 + 4.6(u^2 + v^2))\dfrac{\rho \Omega_m R_m^2 C_m b_m c_m}{8} \\ P_{ind} = T_m v_{im} \\ P_{par} = \left|X_f u\right| + \left|Y_f v\right| + \left|Z_f (w - v_{im})\right| \\ P_{cli} = \begin{cases} -mgw, & w < 0 \\ 0, & w > 0 \end{cases} \\ P_m = P_{pro} + P_{ind} + P_{par} + P_{cli} \end{cases} \tag{11}$$

The symbol R_m signifies the main rotor's radius; C_m denotes the drag coefficient for the blades of the main rotor. b_m and c_m respectively represent the quantity and chord length of the main rotor blades. T_m quantifies the lift produced by the main rotor, while v_{im} is the induced velocity attributable to the main rotor; and X_f Y_f, and Z_f are the components of the lift force generated by the main rotor along the body coordinate system's three axes, respectively.

Newton's third law posits that when the main rotor rotates, the unmanned helicopter's body experiences a reaction torque, which needs to be balanced by the tail rotor. The positive direction of T_t is defined as opposite to the y-axis, corresponding to the direction of Nm.

In the architectural design of the distributed electric tail rotor system for unmanned helicopters, the tilt angle of the tail rotor—defined as the relative angle of the tail rotor blades to the helicopter's flight direction—exerts a significant impact on the aircraft's maneuverability and stability. The unmanned helicopter designed in this thesis utilizes a fixed-pitch, variable-speed structure, where the tilt angle of tail rotor is fixed value and does not adjust with changes in flight conditions. Consequently, the distributed tail rotor can be regarded as a small rotor parallel to the body's symmetrical plane, with its thrust generated through speed adjustments. The distributed electric tail rotor employs four high-performance brushless Direct Current (DC) motors, with each motor's lift proportional to the square of its rotation speed, expressed as follows:

$$T_{ti} = K\omega_{ti}^2, (i = 1, 2, 3, 4) \tag{12}$$

where K is the thrust coefficient. Thus, the total thrust of the distributed electric tail rotor can be represented as:

$$T_t = \sum_{i=1}^{4} T_{ti} = T_{t1} + T_{t2} + T_{t3} + T_{t4} = K\sum_{i=1}^{4} \omega_{ti}^2 \tag{13}$$

In this paper, to simplify the model, it is stipulated that the four motors of the distributed electric tail rotor operate at the same speed. Furthermore, the thrust and torque generated by the distributed electric tail rotor can be accurately described through simplified dynamic equations without involving complex interactions with airflow. This simplified approach allows the study to focus on the torque generated by the distributed electric tail rotor in the yaw direction, which balances the reactive torque produced by the rotation of the main rotor.

Since the forces exerted by the distributed electric tail rotor on the x and z axes are very small, they are considered negligible. Therefore, the forces and torques exerted by the distributed electric tail rotor on the body can be represented as follows:

$$\begin{cases} X_t = 0 \\ Y_t = -T_t \\ Z_t = 0 \\ L_t = Y_t H_t \\ M_t = 0 \\ N_t = -Y_t D_t \end{cases} \tag{14}$$

where T_t denotes the total thrust generated by the distributed electric tail rotor. X_t, Y_t, Z_t are the components of this thrust along the three axes respectively. D_t and H_t represent the radial distance and vertical height of the tail rotor's center point relative to the helicopter's center of gravity. L_t is the

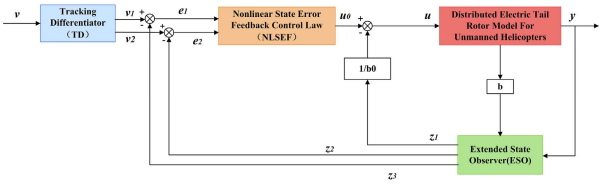

FIGURE 2. Basic structure diagram of active disturbance rejection control.

torque of the distributed electric tail rotor's thrust around the X-axis, specifically the product of the Y-axis of the thrust Y_t and the height H_t from the center point of the tail rotor to the helicopter's center of gravity. M_t is the torque around the Y-axis, which is zero because the thrust direction of the tail rotor is parallel to the Y-axis of the body and the line connecting the center point of the tail rotor to the helicopter's center of gravity is also parallel to the Y-axis. N_t is the torque around the Z-axis, which is the yaw torque generated by the total thrust T_t, specifically represented as the product of the Y-axis of the thrust Y_t and the distance D_t from the center point of the tail rotor to the helicopter's center of gravity.

III. ACTIVE DISTURBANCE REJECTION CONTROLLER DESIGN

A. DESIGN OF THE BASIC ACTIVE DISTURBANCE REJECTION CONTROLLER

In the analysis presented in the second part, we categorize the distributed electric tail rotor system of the unmanned helicopter as a second-order system, detailed as follows:

$$\ddot{y} = f(y, \dot{y}, w(t), t) + bu \tag{15}$$

In this context, $w(t)$ signifies the external disturbance, while $f(y, \dot{y}, w(t), t)$ denotes the body's total disturbance. Furthermore, within this study, y corresponds to the yaw angle, $\dot{y}$ denotes the yaw rate, b represents the system gain and u is the system control quantity. To simplify the explanation, the system's two real-time states are denoted by variables x_1 and x_2, with x_1 corresponding to the yaw angle and x_2 to the yaw rate. This notation facilitates the transformation of (15) into the state-space representation given as (16):

$$\begin{cases} y = x_1 \\ \dot{x}_1 = x_2 \\ \dot{x}_2 = f(x_1, x_2, w(t), t) + bu \end{cases} \tag{16}$$

The core idea of active disturbance rejection control is to estimate and promptly eliminate the total disturbance $f(y, \dot{y}, w(t), t)$ in real-time.

The active disturbance rejection controller consists of three parts: the Tracking Differentiator (TD), the Extended State Observer (ESO), and the Nonlinear State Error Feedback (NLSEF) control law [18]. Fig 2 depicts the fundamental structural diagram of the control system.

The objective of the Tracking Differentiator (TD) is to resolve the problem of discontinuous yaw angle input within the distributed electric tail rotor model. This is achieved by concurrently generating the differential signal of the yaw angle and managing the transition process. The discrete TD is designed according to the following specifications:

$$\begin{cases} x_1(k+1) = x_1(k) + hx_2(k) \\ x_2(k+1) = x_2(k) + hfh \\ fh = fhan(x_1(k) - v(k), x_2(k), r_0, h) \end{cases} \tag{17}$$

The controller's execution period, denoted by h, is a function of the input signal at the k instance, v(k), and the tracking speed parameter, r0. The fast control synthesis function, fhan(), is defined as follows:

$$\begin{cases} d = r_0 h^2 \\ a_0 = x_2 h \\ y = a_0 + x_1 \\ a_1 = \sqrt{d(8\,|y| + d)} \\ a_2 = a_0 + \dfrac{sign(y)(a_1 - d)}{2} \\ s_y = \dfrac{[sign(y+d) - sign(y-d)]}{2} \\ a = a_2 + (-a_2 + y + a_0)sy \\ s_a = \dfrac{[sign(a+d) - sign(a-d)]}{2} \\ fhan = -r_0 sign(a) - r[\dfrac{a}{d} - sign(a)]s_a \end{cases} \tag{18}$$

where r_0 and h are the control parameters of the function.

The primary role of the Extended State Observer (ESO) encompasses the real-time monitoring of the unmanned helicopter's current yaw angle and yaw rate of the unmanned helicopter in real time, while also identifying and compensating for disturbances affecting the aircraft, both internally and externally. ESO is designed as follows:

$$\begin{cases} \varepsilon_1 = z_1(k) - y(k) \\ z_1(k+1) = z_1(k) + h[z_2(k) - \beta_{01}\varepsilon_1] \\ z_2(k+1) = z_2(k) + h[z_3(k) - \beta_{02} fal(\varepsilon_1, a_1, \delta) + bu] \\ z_3(k+1) = z_3(k) - h\beta_{03} fal(\varepsilon_1, a_2, \delta) \end{cases} \tag{19}$$

In (19), $\beta 01$, $\beta 02$, $\beta 03$, $a1$, $a2$, b, δ are the parameters of the controller that need to be adjusted. The expression for the fal function is as follows:

$$fal(e, a, \delta) = \begin{cases} \dfrac{e}{\delta^{(1-a)}} & |e| \le \delta \\ sign(e)\,|e|\,a & |e| > \delta \end{cases} \tag{20}$$

where e represents the input error. a is a constant between 0 and 1. δ is the length of the linear segment interval.

Subtracting the output signal from the tracking differentiator from that of the state observer yields the command error signal e_1 and its differential signal e_2. These signals represent representing the yaw angle deviation and the yaw rate deviation, respectively. These signals are combined in a nonlinear manner to formulate the nonlinear state error feedback control law, which in turn produces the disturbance compensation

control quantity, explicitly designed as follows:

$$\begin{cases} e_1 = v_1(k) - z_1(k) \\ e_2 = v_2(k) - z_2(k) \\ u_0(k) = \beta_1 fal(e_1, a_1, \delta) + \beta_2 fal(e_2, a_2, \delta) \\ u(k) = \dfrac{u_0(k) - z_3(k)}{b_0} \end{cases} \tag{21}$$

where β_1 and β_2 represent the proportional gain and the differential gain, respectively; b_0 is the compensation factor, which is taken as $b_0 = b$ in this paper.

B. IMPROVEMENT OF THE FAL FUNCTION

The fal function exhibits continuous non-smooth characteristics, making it less robust when applied to unmanned helicopter yaw systems with significant unknown disturbances, often requiring the adjustment of numerous fal -related parameters to adapt to the system. Moreover, due to the power function's characteristic of having a high slope near the origin and its inflection points, the presence of measurement noise in the feedback loop can reduce the estimation effectiveness of the extended state observer [19].

In the field of machine learning, smooth functions are generally easier to handle. Therefore, finding smooth approximations for non-smooth functions becomes crucial. For non-smooth functions, common optimization strategies are gradient-based, and employing models that are continuous and smooth in their gradients facilitates optimization. This paper employs the Dirac function to construct a smooth approximation [20], where the Dirac function $\delta(x)$ satisfies:

$$\begin{cases} \forall x \neq 0, \delta(x) = 0 \\ \delta(0) = \infty \\ \int_{-\infty}^{\infty} \delta(x)dx = 1 \end{cases} \tag{22}$$

In the typical case, $\delta(x)$ is regarded as a continuous probability density function with its sampling space being all real numbers R. It is conventional to define the probability as zero outside $x = 0$, which implies that the mean and variance are both zero. Upon sampling from this distribution, the resulting value is zero, thereby satisfying the following identity:

$$\int_{-\infty}^{\infty} f(x)\delta(x)dx = f(0) \tag{23}$$

Or

$$\int_{-\infty}^{\infty} f(y)\delta(x-y)dy = f(x) \tag{24}$$

(23) and (24) are equivalent and represent important properties of the Dirac function.

Seeking a smooth approximation $\mu(x) = \delta(x)$ for $\delta(x)$, based on the important properties of the Dirac function, we can obtain:

$$s(x) = \int_{-\infty}^{\infty} f(y)\mu(x-y)dy \approx f(x) \tag{25}$$

The key to constructing a smooth approximation of f(x) using the smooth approximation of the Dirac function is that $\mu(x)$ is smooth, which implies that s(x) is also smooth. This means that s(x) is a smooth approximation of $\mu(x)$.

There are various forms of smooth approximations to the Dirac function. This study selects the following form:

$$\delta(x) = \lim_{\theta \to 0} \frac{e^{-\frac{x^2}{2\theta^2}}}{\sqrt{2\pi}\theta} \tag{26}$$

By leveraging (26) and capitalizing on the critical attributes of the Dirac function, we enhance the smoothed approximation of the fal function, hereby termed as newfal(·). The following section will articulate this improved approximation.

$$newfal(\cdot) = \int_{-\infty}^{\infty} \frac{e^{-\frac{x^2}{2\theta^2}}}{\sqrt{2\pi}\theta} fal(e, a, \delta)d\delta \tag{27}$$

Within the control system of the unmanned helicopter's distributed electric tail rotor, external environmental disturbances affect system performance. Compared to traditional fal function designs, an improved fal function constructed using the Dirac function exploits its smooth characteristics as well as its continuity and smoothness across the entire function domain, resulting in lower rate changes around the origin and superior disturbance rejection, thereby enhancing system stability. Furthermore, the smooth approximation of this function further ensures the continuity of control signal changes, improving control precision and response speed.

Fig 3 presents a simulation graph that contrasts the improved fal function against the conventional fal function near the origin.

As evident from Fig 3, the improved fal function demonstrates enhanced smoothness around the origin compared to its traditional counterpart. Therefore, the improved fal function effectively avoids high-frequency oscillations caused by excessive gain, exhibiting better smoothness and convergence. Additionally, the improved fal function still maintains the characteristic of "large error, small gain; small error, large gain" [21]. Applying the improved fal function to the Extended State Observer significantly enhances the observer's capability, yielding better control effects for the distributed electric tail rotor system.

C. CASCADED ACTIVE DISTURBANCE REJECTION CONTROL DESIGN

The distributed electric tail rotor's yaw channel in the unmanned helicopter employs a cascaded active disturbance rejection control strategy. This system feeds the yaw channel's output angular velocity into the inner loop's extended state observer and relays yaw angle data to the outer loop's extended state observer. The MPU6050 attitude sensor measures the yaw rate and yaw angle of the unmanned helicopter's distributed electric tail rotor. Figure 4 depicts the architecture of the dual-loop distributed electric tail rotor

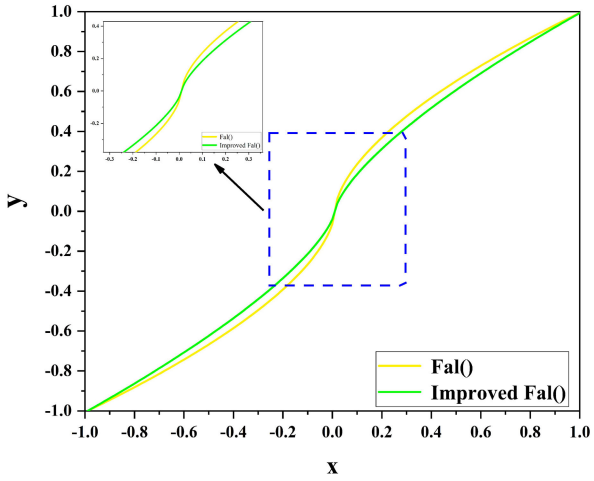

FIGURE 3. Comparison chart of simulated curves between improved and traditional fal functions.

yaw channel, which employs a cascaded active disturbance rejection control strategy.

IV. DESIGN OF THE MAIN CONTROL BOARD AND SOFTWARE FOR THE DISTRIBUTED ELECTRIC TAIL ROTOR TEST STAND

A. CONSTRUCTION OF THE DISTRIBUTED ELECTRIC TAIL ROTOR TEST STAND

To verify the feasibility of this method, a set of unmanned helicopter distributed electric tail rotor test stand was independently designed using SolidWorks and CATIA software. The test stand mainly consists of the main rotor and distributed electric tail rotor. Each component is equipped with high-performance brushless DC motors, electronic speed controllers, and quality blades. Figure 5 depicts the actual test stand constructed.

B. MAIN CONTROL BOARD HARDWARE DESIGN

The hardware of the main control board employs the STM32F407 minimal system board as the core processing unit and includes a DC stabilized power supply module, an MPU6050 module, a wireless serial port module, five PWM output modules, a TFT screen module, a buzzer module, a button module, an LED indicator module, an infrared module, and a USB power supply module. Figure 6 illustrates the hardware design structure of the aforementioned main control board.

The DC voltage stabilizer module is responsible for providing a stable power output to the distributed electric tail rotor control system, ensuring that all modules operate safely at the ideal voltage. The MPU6050 module communicates with the STM32F407, transmitting real-time data on the unmanned helicopter's yaw angle and yaw rate, and displays the data on a TFT screen to assess flight status and the impact of external disturbances. The infrared remote control module uses infrared sensing technology to convert signals

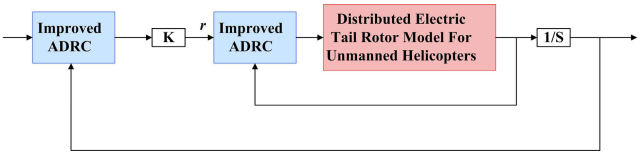

FIGURE 4. Structure diagram of the yaw channel with cascaded active disturbance rejection control.

FIGURE 5. Overall physical image of the unmanned helicopter distributed electric tail rotor test stand.

into electrical signals, facilitating the adjustment of the main rotor's speed. The PWM output module for the main rotor and distributed electric tail rotor receives PWM signals from the STM32F407, controlling the operation of brushless DC motors, ensuring the system responds promptly.

Fig 7 shows the actual PCB of the main control board circuit hardware:

C. MAIN CONTROL BOARD HARDWARE DESIGN

Utilizing the Keil5 integrated development environment, the main control board is first initialized upon power-up, then the STM32F407 collects sensor data and communicates with the ground station via serial port. After receiving the data, the ground station is responsible for real-time data output and graph drawing, enhancing the system debugging and optimization efficiency. In this study, the ground station software "Anonymous Ground Station" is selected. Through PWM channels, the calculation results are converted into precise tail rotor motor control signals, thus adjusting the unmanned helicopter's yaw channel.

V. VERIFICATION AND RESULT ANALYSIS

A. SIMULATION VERIFICATION

In order to assess the efficacy of the refined ADRC control approach, we developed a mathematical model of the unmanned helicopter, equipped with distributed electric tail rotors, using simulation software. Subsequently, yaw channel tracking tests were performed and the results were benchmarked against those obtained using traditional ADRC

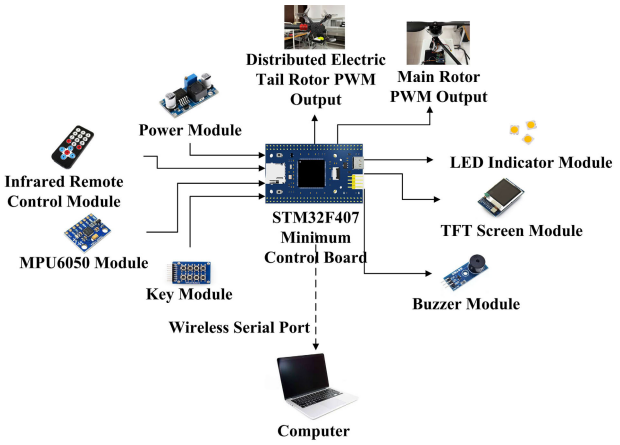

FIGURE 6. Main control board circuit hardware design diagram.

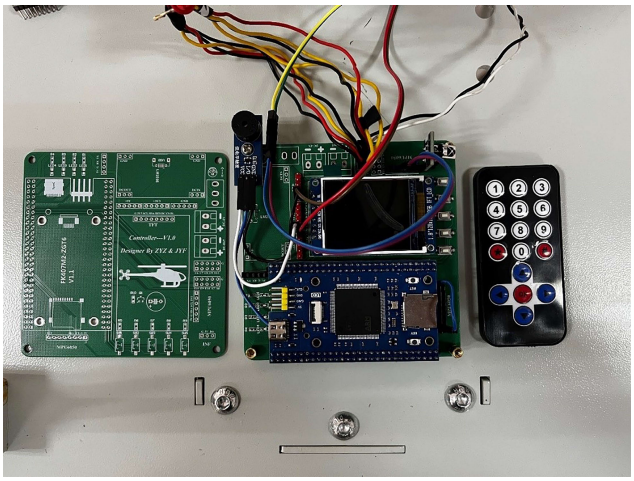

FIGURE 7. Actual PCB image of main control board circuit hardware.

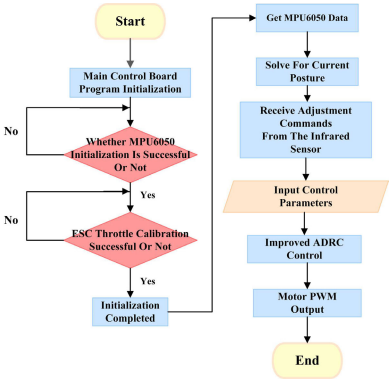

FIGURE 8. Software flowchart.

control methods. The parameters of the unmanned helicopter are shown in Table 1.

This study utilizes an ADRC algorithm based on an improved fal function to construct a nonlinear combination function, with adjustable parameters including r_0, h, β_{01}, β_{02}, β_{03}, δ , b, θ, β_1, β_2 , a_1 , a_2 , b_0. Employing a cascaded ADRC approach, this research necessitates distinct parameter tuning for the ADRC's inner and outer loops. The improved ADRC parameters are shown in Table 2.

Design a simulation test for clear weather outdoor conditions without external wind disturbances to compare and validate the tracking performance of the improved ADRC control method versus the traditional ADRC control method on the yaw angle and yaw rate of an unmanned helicopter equipped with a distributed electric tail rotor. The experiment set the initial yaw angle of the unmanned helicopter to 0° with a sampling period of 0.01s. At the 4s mark, a 10° rectangular wave with a 40% duty cycle was introduced to simulate a 10° left turn of the body. After returning to neutral, at 9s, a 25° rectangular wave with a 40% duty cycle was introduced to simulate a 25° left turn. After returning to neutral, at 14s, a 5° rectangular wave with a 40% duty cycle was introduced to simulate a 5° right turn. After returning to neutral, at 19s, a 20° rectangular wave with a 40% duty cycle was introduced to simulate a 20° right turn. Fig 10 illustrates the yaw angle tracking curve for the unmanned helicopter.

From Fig 10, it is evident that both methods can quickly track the desired yaw angle. However, traditional ADRC exhibits some degree of overshoot. Compared to traditional ADRC, the improved ADRC has less overshoot, with a maximum reduction of 90% in overshoot and a 42.86% savings in adjustment time, resulting in shorter adjustment times and faster responses. Both methods exhibit slight oscillations, likely due to some coupling between the channels of the unmanned helicopter. Fig 11 shows the yaw rate tracking curve for the unmanned helicopter.

After the body undergoes deflection, the distributed electric tail rotor can quickly respond to maintain the stability of the body, as demonstrated by the rapid convergence of the yaw rate to 0°. Fig 11 reveals that both methods can quickly converge the yaw rate to 0°. However, the figure clearly shows that traditional ADRC exhibits overshoot. In comparison, the improved ADRC reduces overshoot by up to 89.47% and shortens adjustment time by 56.82%, proving a reduction in overshoot and a shorter adjustment time. This simulation result confirms that, compared to ADRC control using the traditional fal function, the ADRC control strategy with the improved fal function has superior control capability and stability performance.

Unmanned helicopters are commonly used in complex environments with external wind disturbances, making it necessary to conduct simulation tests in gusty conditions. The gust model simulates sudden changes in wind speed in natural environments, with a design delineated as follows:

$$V_z = \begin{cases} 0 & (t < t_z) \\ \dfrac{V_{zmax}}{2}\left\{-\cos\left[2\pi\left(\dfrac{t-t_z}{T_z}\right)\right]+1\right\} & (t_z \le t \le t_z + T_z) \\ 0 & (t > t_z + T_z) \end{cases} \tag{28}$$

TABLE 1. Unmanned helicopter parameters.

Symbol	Parameters	Values
m	unmanned helicopter body weight	7.5(kg)
R_m	main rotor radius	0.716(m)
C_m	main rotor blade drag coefficient	0.055
b_m	number of main rotor blades	2
c_m	main rotor blade chord length	0.12(m)
I_{zz}	moment of inertia of unmanned helicopter about Oz axis	0.3408(kg • m^2)
K	thrust coefficient of distributed electric tail rotor	2
D_t	distance from the center point of the distributed electric tail rotor to the center of gravity of the body	0.796(m)
H_t	height of the distributed electric tail rotor's center point relative to the body's center of gravity	0.235(m)

TABLE 2. Simulation tests for improved ADRC parameters.

Link	Symbol	Inner Loop Values	Outer Loop Values
TD	r_0	20	20
	h	0.05	0.05
ESO	β_{01}	70	130
	β_{02}	400	600
	β_{03}	900	1
	δ	0.1	0.1
	b	39	39
	a_1	0.5	0.5
	a_2	0.25	0.25
	θ	2	2
NLSEF	β_1	5	0.8
	β_2	4	0.2
	a_1	0.5	0.5
	a_2	0.25	0.25
	b_0	39	39

where V_z denotes the velocity of the gust wind, quantified in meters per second; V_{zmax} signifies the gust's maximum intensity, also measured in meters per second; t_z marks the onset of the gust, recorded in seconds; T_z delineates the duration of the gust cycle, in seconds. For this test, the gust starts at $t_z = 7$s, with a cycle of $T_z = 5$s and a maximum peak of $V_{zmax} = 1.5$m/s. The trajectory of the yaw angle response of the unmanned helicopter under these specified gust conditions is depicted in Figure 11.

As shown in Figure 11, following the gust disturbance at the 7th second, both methods performed well in tracking the desired yaw angle, with the yaw angle deviation not exceeding 1.14°, thus maintaining the stability of the airframe. However, traditional ADRC exhibited greater overshoot. In a close-up view, the improved ADRC had significantly less overshoot, reducing by 83%, and the yaw angle error was reduced by 2%. These simulation results demonstrate that under the influence of external gusts, the ADRC control strategy using the improved fal function offers superior robustness and stability compared to the traditional fal function control strategy.

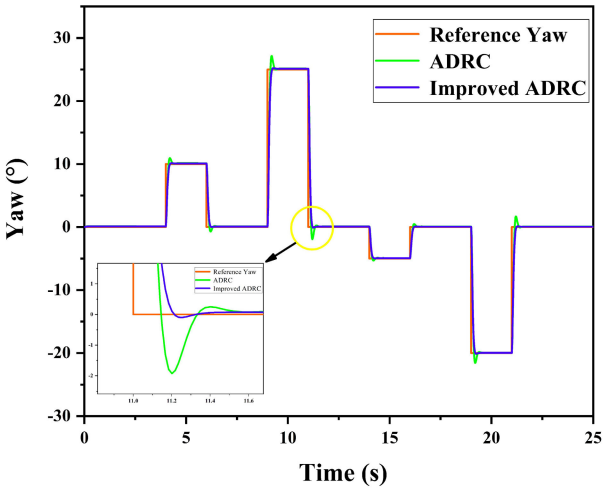

FIGURE 9. Comparative chart of yaw angle tracking control in an environment free from external wind disturbances.

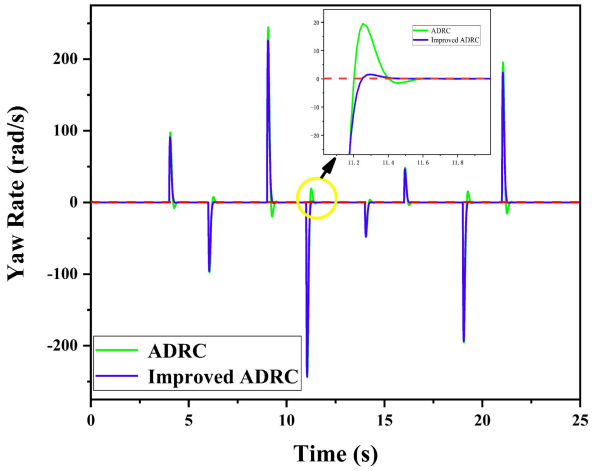

FIGURE 10. Comparative chart of yaw angle rate tracking control in an environment free from external wind disturbances.

B. TESTING AND DATA ANALYSIS OF DISTRIBUTED ELECTRIC TAIL ROTOR TEST STAND

During the test bench trials, parameters were tuned and optimized to determine the most suitable ADRC parameters for testing the distributed electric tail rotor, as detailed in Table 3.

After securing the test stand, assembling the hardware, and completing the wiring, power is supplied to both the main rotor motor and the distributed tail rotor motors. In the design of the distributed electric tail rotor, motor 1 and motor 3 are set to rotate counterclockwise, while motor 2 and motor 4 rotate clockwise, with respective installation of standard and reverse propellers.

The first test is to verify whether the unmanned helicopter can quickly reach a self-stabilizing state upon startup. Controlled by an infrared remote controller for start-stop operations, upon starting, the main rotor motor rotates counterclockwise, generating a clockwise torque on the body, leading to deflection. This experiment aims to verify whether

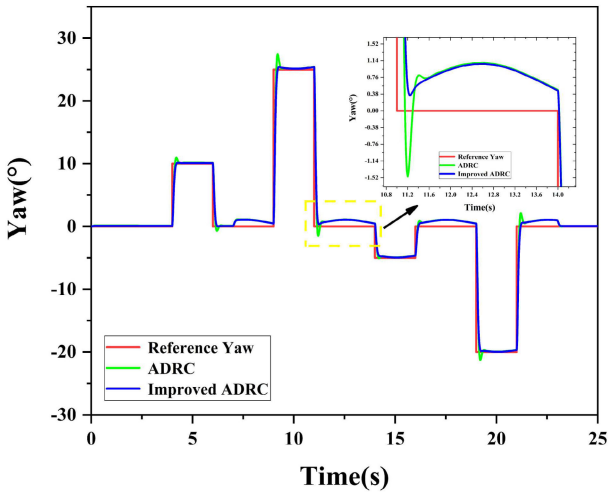

FIGURE 11. Comparison chart of yaw angle tracking control in a gusty environment.

TABLE 3. Test bench trials of improved ADRC parameters.

Link	Symbol	Inner Loop Values	Outer Loop Values
TD	r_0	20	20
	h	0.05	0.05
ESO	β_{01}	65	135
	β_{02}	430	640
	β_{03}	850	4
	δ	0.1	0.1
	b	42	50
	a_1	0.5	0.5
	a_2	0.25	0.25
	θ	2	2
NLSEF	β_1	6	1.5
	β_2	4	0.5
	a_1	0.5	0.5
	a_2	0.25	0.25
	b_0	42	50

the distributed electric tail rotor can produce sufficient counterclockwise thrust using an improved ADRC control algorithm to counteract the torque generated by the main rotor, quickly achieving a self-stabilizing state upon startup. Fig 12 presents the data from the startup self-stabilization test.

Fig 12 clearly illustrates that three start-stop tests occurred at 3.4 s, 6.7 s, and 9.5 s respectively. Following each startup, the rotation of the main rotor induced a counter-torque, resulting in the body's deflection and significant fluctuations in the yaw angle data curve. Using the improved ADRC control algorithm, the yaw angle can be maintained at its original position, and the yaw rate quickly converges to 0, achieving self-stabilization upon startup. It is clearly seen in the figure that in the three startup tests, the body reached a stable state in 1.53 s, 2.338 s, and 1.828 s respectively. This demonstrates that the improved ADRC control method can achieve self-stabilization of the body upon startup with excellent effect.

As shown in Figure 13, the green curve represents the PWM output values of the distributed electric tail rotor obtained through the improved ADRC control algorithm. At 3.4 s, both the main rotor and the distributed electric tail rotor start simultaneously, with the tail rotor rotating at low speed. As the main rotor speed gradually increases, causing the body to yaw, the distributed electric tail rotor responds quickly at 4 s, with a sharp increase in PWM output, instantly counteracting the reactive torque from the main rotor. At 4.6 s, the body approaches a self-stabilizing state, the yaw angle converges to 0°, and the distributed electric tail rotor maintains high-speed output to keep the body stable. When the body's yaw angle undergoes another sharp deviation, the PWM output of the distributed electric tail rotor first decreases and then increases, achieving body stabilization. The chart clearly demonstrates that the improved ADRC control method performs excellently in the process of achieving body stabilization.

Subsequently, selecting the moment of the body's stable state as the test point, the main rotor's rotational speed is changed using the remote control keys, thereby altering the counter-torque generated on the body. This experimental setup aims to assess whether the distributed electric tail rotor can effectively neutralize the counter-torque from the main rotor, thus preserving the body's stability. Fig 14 presents the torque resistance test data for the distributed electric tail rotor.

Fig 14 reveals that the main rotor motor initiates at a speed of 450 rpm. At the 1.3s mark, the speed of the main rotor quickly increases to 630 rpm, causing the body to deflect due to the counter-torque generated by the rotation of the main rotor. At this moment, both the yaw angle and yaw rate experience significant fluctuations. With the improved ADRC control method, the yaw angle is maintained at its original position, and the yaw rate quickly converges to 0, with a convergence time of 1.518s. After stabilizing, the speed of the main rotor is gradually increased at the 3.5s mark until it reaches 735 rpm at 5.9s. During this process, the yaw angle remains at its original position, and the yaw rate experiences minimal jitter, not exceeding 0.4%. A second test is conducted at the 6.1s mark, gradually increasing the main rotor speed after restarting and achieving self-stability at the 8s mark, until the main rotor speed increases to 730 rpm at the 10s mark, then decreasing the main rotor speed at the 10.6s mark until it reaches 640rad/s at 12.7s, and then completing another increase-decrease process. Throughout this process, the yaw angle remains at its original position, and the yaw rate jitter does not exceed 0.5%. The test results show that, whether increasing or decreasing the main rotor speed, the distributed electric tail rotor can automatically and quickly adjust the speed of the four tail rotor motors using the improved ADRC control method, effectively counteracting the counter-torque generated by the main rotor. This result validates that the improved ADRC control algorithm can effectively maintain the stability of the unmanned helicopter's yaw channel after changing the main rotor speed.

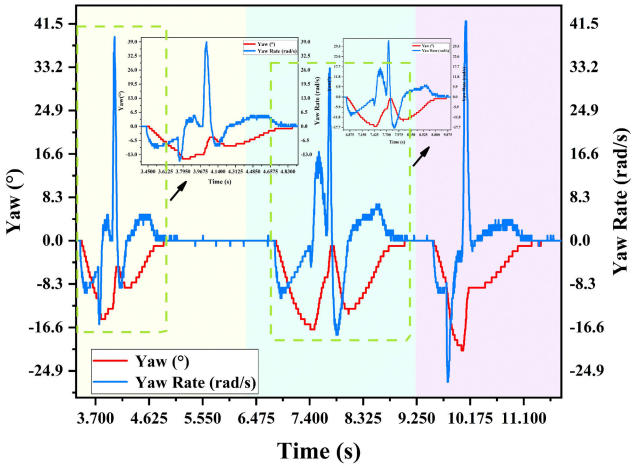

FIGURE 12. Startup self-stabilization test data chart.

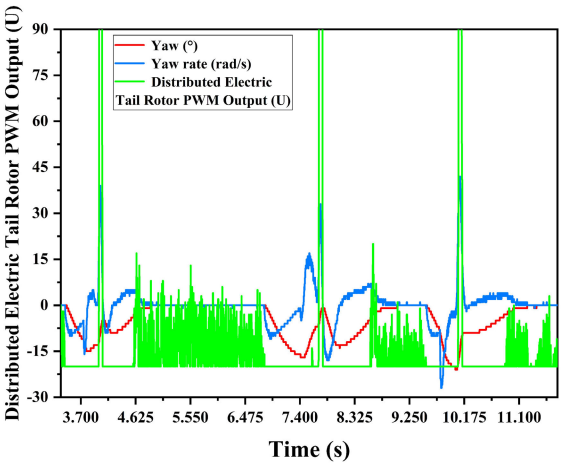

FIGURE 13. Startup self-stabilization distributed electric tail rotor PWM output data chart.

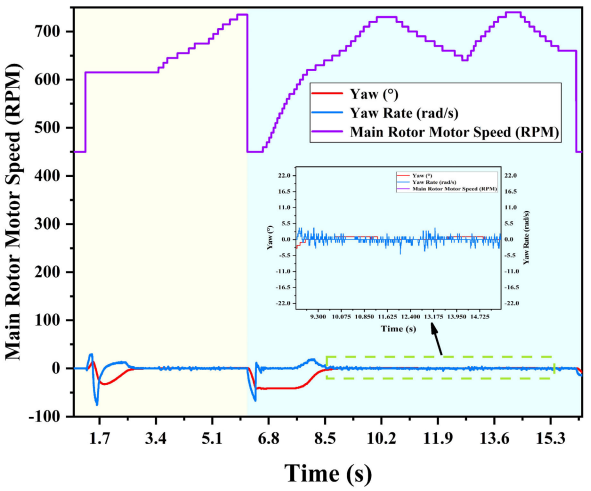

FIGURE 14. Distributed electric tail rotor torque resistance test data chart.

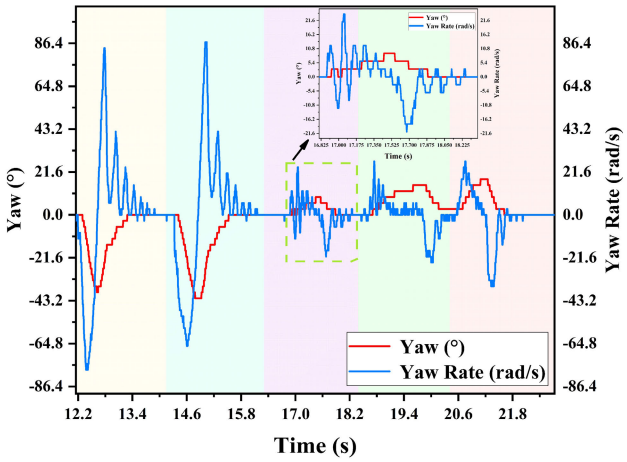

FIGURE 15. Yaw disturbance correction test data chart.

Next, the position at which the body is in a stable state is selected as the test point for the yaw disturbance correction test. This test involves applying a yaw-direction disturbance to change the body's yaw direction, observing whether the distributed electric tail rotor can immediately respond and correct the body back to the test point, quickly achieving a balanced and stable state. Fig 15 displays the data from the yaw disturbance correction test.

In the flight control of unmanned helicopters, disturbances in the yaw channel are typically caused by external wind forces or asymmetric loads, which instantaneously alter the helicopter's yaw angle and yaw rate. To counter such disturbances, this design of the unmanned helicopter, termed ''fixed-pitch, variable-speed,'' employs a distributed electric tail rotor. By swiftly adjusting the motor speed to increase the thrust generated by the tail rotor, the external forces caused by disturbances are counteracted, thus reducing the yaw rate and rapidly converging the yaw angle to 0°, returning the body to the target position. As the distributed electric tail rotor continuously adjusts, the yaw angle and yaw rate gradually stabilize, ultimately restoring a self-stabilizing equilibrium state.

Fig 15 clearly illustrates that a series of five yaw disturbances were executed. The red line data above the y-axis zero point represents disturbances applied to the right of the body, while the red line data below the zero point indicates disturbances applied to the left. Selecting the data within the squares in the graph as an instance of yaw disturbance, a rightward disturbance was applied to the body at 16.87s, causing a 9° rightward deflection of the yaw angle. The angle curve showed significant fluctuations, and the yaw rate converged to 0 after an adjustment time of 1.406s. The test results show that after each disturbance applied to the body's yaw, the distributed electric tail rotor can quickly adjust using the improved ADRC, enabling the body to quickly correct and maintain a stable state. This demonstrates the excellent anti-interference capability of the improved ADRC control

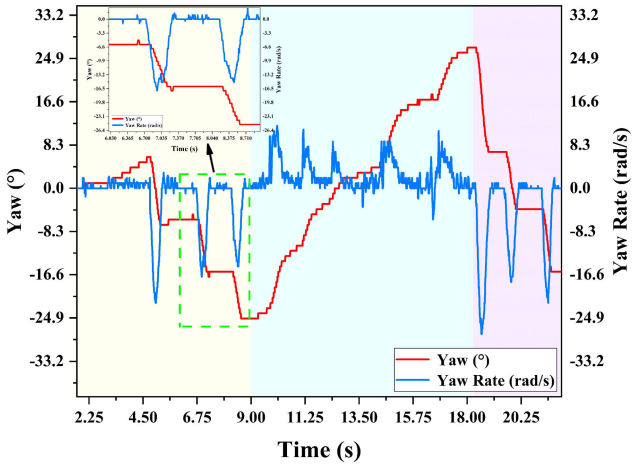

FIGURE 16. Fixed yaw disturbance test data chart.

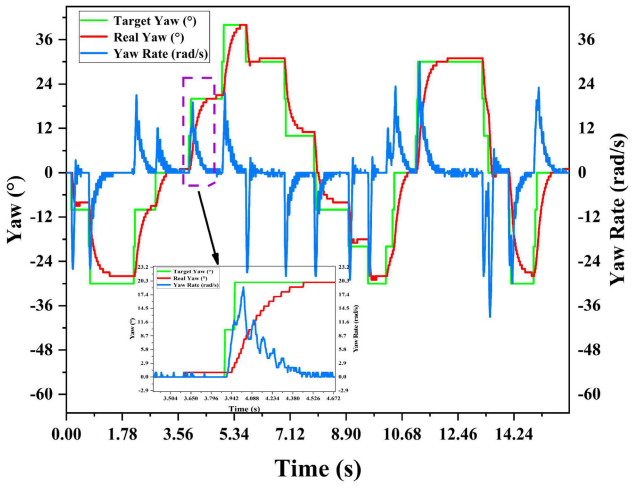

FIGURE 17. Yaw angle tracking test data chart.

method, exhibiting outstanding performance in the unmanned helicopter yaw channel disturbance correction test.

Subsequent tests were conducted for fixed yaw disturbances. This test involved applying a disturbance to the body, causing a change in the yaw direction, and observing whether the distributed electric tail rotor could quickly respond, enabling the body to rapidly achieve a new balanced and stable state after changing the yaw direction. Fig 16 displays the data from the fixed yaw disturbance examination.

Figure 16 illustrates that the body experienced multiple disturbances from various directions, leading to notable fluctuations in the yaw angle curve. Selecting the data within the squares in the graph, two disturbances to the left were applied to the fuselage at 6.6s and 8.2s, causing leftward deflections of the yaw angle by 10.2° and 9°, respectively. After each disturbance deflection, the yaw rate quickly converged to zero, with convergence times of 0.638 s and 0.64 s respectively. The experimental data show that after each perturbation, the distributed electric tail rotor can achieve rapid stabilization of the airframe after the perturbation by using the improved ADRC control algorithm, and this method helps to maintain the attitude stability of the unmanned helicopter.

Finally, a yaw angle tracking test is conducted. The position of the body in a stable state is selected as the test point. By operating the remote control keys, the body is turned to a preset angle. The test observes whether the distributed electric tail rotor can quickly track the yaw angle and swiftly and accurately adjust the body to the target angle, achieving a stable state in a short time. Fig 17 shows the data for the yaw angle tracking test.

Fig 17 clearly demonstrates that the body received several specified angle yaw commands, with deflection angles varying from 10° to 30°. Selecting the data within the squares in the graph as an instance of a yaw angle tracking test, at 3.6s, a command was given for the yaw angle to deflect 20° to the right. The electric tail rotor quickly tracked the target angle within 0.576 seconds, without any overshoot. Additionally, the yaw rate was quickly adjusted and converged to 0 within 0.578 seconds, with a slight jitter in the yaw rate after the body stabilized, not exceeding 0.95%. The experimental data demonstrate that while the body undergoes a specified angle deflection, the distributed electric tail rotor, applying the improved ADRC control algorithm, can quickly track the target angle. These results fully attest to the superior performance of the improved ADRC control algorithm in rapid response capability and precise control of the unmanned helicopter's yaw channel.

VI. CONCLUSION

This paper has developed and designed a distributed electric tail rotor yaw channel controller for unmanned helicopters based on ADRC control. A mathematical model of an unmanned helicopter with a distributed electric tail rotor and an improved fal function was constructed, addressing the issue of excessive error gain in the expanded state observer that causes overshoot and oscillation. The hardware, software, and a test bench for the unmanned helicopter with a distributed electric tail rotor have been designed and constructed. Simulation tests have proved that the improved ADRC control is enhanced; multiple test bench trials have confirmed that the improved ADRC control method exhibits exceptional performance in the yaw channel control of unmanned helicopters with distributed electric tail rotors.

REFERENCES

[1] X.-Z. Tang, G.-J. Chen, and Y. Fu, "Comprehensive evaluation technique research on the conceptual scheme of distributed electric drive anti-torque system for light helicopters," *Aeronaut. Sci. Technol.*, vol. 34, no. 2, pp. 56–63, 2023, doi: 10.19452/j.issn1007-5453.2023.02.008.

[2] Z.-X. Jian, X.-Z. Tang, and G.-J. Chen, "Helicopter electric tail rotor technology development and prospects," *Helicopter Technique*, vol. 3, pp. 58–64, Jan. 2021, doi: 10.3969/j.issn.1673-1220.2021.03.011.

[3] A. H. Mary, A. H. Miry, and M. H. Miry, "Design robust H_∞-PID controller for a helicopter system using sequential quadratic programming algorithm," *Zhōngguó gōngchéng xuékōn*, vol. 45, no. 8, pp. 688–696, Oct. 2022, doi: 10.1080/02533839.2022.2126401.

[4] D. Tang, J. Zhao, and H. Li, "An improved teaching-learning-based optimization algorithm with memetic method for global optimization," *Int. J. Advancements Comput. Technol.*, vol. 5, no. 9, pp. 942–949, May 2013, doi: 10.4156/ijact.vol5.issue9.112.

[5] K. Rathod and S. J. Mija, "Robust control of 2-DoF helicopter system in presence of unmatched disturbances & actuator faults," in *Proc. 2nd Int. Conf. Intell. Technol. (CONIT)*, Hubli, India, Jun. 2022, pp. 1–7, doi: 10.1109/CONIT55038.2022.9848199.

[6] A. Chaudhary, "Axis control of a nonlinear helicopter model using intelligent controller," in *Proc. Int. Conf. Advancement Technol. (ICONAT)*, Goa, India, Jan. 2023, pp. 1–6, doi: 10.1109/ICONAT57137.2023.10080707.

[7] J. Zhu, X. Sun, Q. Zhang, and C. Hao, "Attitude angle compound controller design for TREX 700L electric unmanned helicopter," in *Proc. 34th Chin. Control Decis. Conf. (CCDC)*, Hefei, China, Aug. 2022, pp. 3236–3241, doi: 10.1109/CCDC55256.2022.10033810.

[8] S. Wang, "Approximation-free control for nonlinear helicopters with unknown dynamics," *IEEE Trans. Circuits Syst. II, Exp. Briefs*, vol. 69, no. 7, pp. 3254–3258, Jul. 2022, doi: 10.1109/TCSII.2022.3142426.

[9] M. I. Uddin, R. K. Sharma, R. Kumar, and E. Deenadayalan, "Adaptive backstepping control of 2-DOF helicopter system under parametric uncertainty," in *Proc. Int. Conf. Power, Instrum., Control Comput. (PICC)*, Thrissur, India, Apr. 2023, pp. 1–6, doi: 10.1109/PICC57976.2023.10142491.

[10] S. M. Schlanbusch and J. Zhou, "Adaptive control of an uncertain 2-DOF helicopter system with input delays," in *Proc. 49th Annu. Conf. IEEE Ind. Electron. Soc.*, Singapore, Oct. 2023, pp. 1–6, doi: 10.1109/iecon51785.2023.10312591.

[11] F. Yacef, N. Benkhaled, L. Benhammouda, L. Melkou, L. Degaa, N. Rizoug, and M. Belhocine, "Adaptive intelligent control of 2-DOF helicopter system," in *Proc. 9th Int. Conf. Control, Decis. Inf. Technol. (CoDIT)*, Rome, Italy, Jul. 2023, pp. 2734–2739, doi: 10.1109/codit58514.2023.10284242.

[12] L. Sun and F. You, "Machine learning and data-driven techniques for the control of smart power generation systems: An uncertainty handling perspective," *Engineering*, vol. 7, no. 9, pp. 1239–1247, Sep. 2021, doi: 10.1016/j.eng.2021.04.020.

[13] L. Sun, W. Xue, D. Li, H. Zhu, and Z.-G. Su, "Quantitative tuning of active disturbance rejection controller for FOPTD model with application to power plant control," *IEEE Trans. Ind. Electron.*, vol. 69, no. 1, pp. 805–815, Jan. 2022, doi: 10.1109/TIE.2021.3050372.

[14] W.-H. Wu, *Helicopter Flight Control System*. Xi'an, China: Northwestern Polytechnical Univ. Press, 2020.01.

[15] C.-E. Zhong, "Modeling and simulation of helicopter 3-axis attitude stabilization loop," *China Sci. Technol. Inf.*, no. 9, pp. 25–26, 2018, doi: 10.3969/j.issn.1001-8972.2018.09.005.

[16] T. A. Shams, S. I. A. Shah, A. Shahzad, A. Javed, and K. Mehmod, "Experimental investigation of propeller induced flow on flying wing micro aerial vehicle for improved 6DOF modeling," *IEEE Access*, vol. 8, pp. 179626–179647, 2020, doi: 10.1109/ACCESS.2020.3026005.

[17] T. A. Shams, S. I. A. Shah, A. Javed, and S. H. R. Hamdani, "Airfoil selection procedure, wind tunnel experimentation and implementation of 6DOF modeling on a flying wing micro aerial vehicle," *Micromachines*, vol. 11, no. 6, p. 553, May 2020, doi: 10.3390/mi11060553.

[18] Z.-Y. Heng, "Research on helicopter electric tail rotor control technology based on ADRC," Ph.D. dissertation, Univ. Electron. Sci. Technol. China, 2021, doi: 10.27005/d.cnki.gdzku.2021.004105.

[19] S. Tang, L. Mao, G. Liu, and W. Wang, "Active disturbance rejection control design of the yaw channel for a small-scale helicopter based on backstepping," in *Proc. Chinese Control Conf. (CCC)*, Jul. 2019, pp. 8073–8078, doi: 10.23919/chicc.2019.8865238.

[20] B. Zhu, *Introduction to Self-Improvement Control*. Beijing, China: Beihang Univ. Press, 2017.

[21] X. Ren, W. Yang, W.-H. Cheng, and J. Liu, "LR3M: Robust low-light enhancement via low-rank regularized retinex model," *IEEE Trans. Image Process.*, vol. 29, pp. 5862–5876, 2020, doi: 10.1109/TIP.2020.2984098.

[22] K. Biswas, S. Kumar, S. Banerjee, and A. K. Pandey, "SAU: Smooth activation function using convolution with approximate identities," in *Proc. Eur. Conf. Comput. Vis.* Cham, Switzerland: Springer, 2022, pp. 313–329.

[23] L. Xu, C. Lu, Y. Xu, and J. Jia, "Image smoothing via L_0 gradient minimization," *ACM Trans. Graph.*, vol. 30, no. 6, pp. 1–12, Dec. 2011, doi: 10.1145/2070781.2024208.

[24] Y.-M. Song, B.-A. Hu, and K. Yin, "Key technology analysis of helicopter tail rotor electric drive system," *Aerosp. Power*, no. 1, pp. 24–26, 2020.

[25] B. Zhou, "Research on nonlinear modeling and control methods for small unmanned helicopters," Ph.D. dissertation, Nat. Univ. Defense Technol., 2019, doi: 10.27052/d.cnki.gzjgu.2019.000362.

[26] I. Chuckpaiwong and A. Boekfah, "Low-cost educational feedback control system: Helicopter tail rotor for yaw control," in *Proc. IEEE 7th Int. Conf. Ind. Eng. Appl. (ICIEA)*, Apr. 2020, pp. 266–270, doi: 10.1109/iciea49774.2020.9102005.

[27] P. Tang, "Research on helicopter tail rotor electric drive and yaw control methods," Ph.D. dissertation, Univ. Electron. Sci. Technol. China, 2021, doi: 10.27005/d.cnki.gdzku.2021.005034.

[28] L. Ding, "Flight dynamics control and experimental study of small unmanned helicopter," Ph.D. dissertation, Nanjing Univ. Aeronaut. Astronaut., 2016.

[29] X. Shi, Y. Cheng, C. Yin, S. Zhong, X. Huang, K. Chen, and G. Qiu, "Adaptive fractional-order SMC controller design for unmanned quadrotor helicopter under actuator fault and disturbances," *IEEE Access*, vol. 8, pp. 103792–103802, 2020, doi: 10.1109/ACCESS.2020.2998698.

[30] I. Ullah and H.-L. Pei, "Fixed time disturbance observer based sliding mode control for a miniature unmanned helicopter hover operations in presence of external disturbances," *IEEE Access*, vol. 8, pp. 73173–73181, 2020, doi: 10.1109/ACCESS.2020.2987960.

[31] D. J. Almakhles, "Robust backstepping sliding mode control for a quadrotor trajectory tracking application," *IEEE Access*, vol. 8, pp. 5515–5525, 2020, doi: 10.1109/ACCESS.2019.2962722.

[32] L. Ding, R. Ma, and W. T. Shan, "Linear self-immunity control of heading for small unmanned helicopters," *Trans. Chin. Soc. Agricult. Machinery*, vol. 48, no. 5, pp. 22–27, 2017, doi: 10.6041/j.issn.1000-1298.2017.05.002.

[33] S. Shen and J. Xu, "Trajectory tracking active disturbance rejection control of the unmanned helicopter and its parameters tuning," *IEEE Access*, vol. 9, pp. 56773–56785, 2021.

[34] S. Topczewski, J. Narkiewicz, and P. Bibik, "Helicopter control during landing on a moving confined platform," *IEEE Access*, vol. 8, pp. 107315–107325, 2020, doi: 10.1109/ACCESS.2020.3000294.

QING-XIN ZHANG was born in Hebei, China, in 1970. He received the M.S. degree in control theory and control engineering from Liaoning Technical University, Fuxin, China, in 1996, and the Ph.D. degree in electrical theory and new technology from Shenyang University of Technology, Shenyang, China, in 2006.

He is the Dean of Liaoning General Aviation Academy (LGAA) as well as the Director of the Key Laboratory of General Aviation of Shenyang Aerospace University. He has led several major research projects and published over 60 academic papers in journals, such as the *Journal of China Electrical Engineering* and *Robotics* and at significant international conferences related to IEEE. He also owns one monograph and more than ten patents. His research interests mainly include intelligent information acquisition and processing, fault diagnosis, general aviation aircraft state detection and evaluation, intelligent robot control and simulation, intelligent instruments, and control systems.

Dr. Zhang is a distinguished young backbone teacher in Liaoning Province, a leading talent in Shenyang City, the lead lecturer of the "Fundamentals of Control Engineering" course in Liaoning Province, a member of the Science Popularization Committee of the Artificial Intelligence Society, and the Vice-Chairperson of the Automatic Control Committee of the Liaoning Society of Aeronautics and Astronautics.

YUN-FENG JI was born in Anshan, Liaoning, China, in 2000. He received the Bachelor of Engineering degree in the Internet of Things engineering from Liaoning University of Science and Technology, in 2022. He is currently pursuing the master's degree in control science and engineering with Shenyang Aerospace University.

Since 2023, his primary research direction has been the attitude control of unmanned helicopters, including studies on intelligent algorithm control of helicopter attitudes and control research on helicopter electric tail rotors. He independently built a test stand for distributed electric tail rotor control and currently holds one patent.

Mr. Ji has received a number of awards, including the National Scholarship and the Star of Self-improvement for Chinese University Students.

FENG WANG was born in Chaoyang, Liaoning, China, in 1977. He received the Bachelor of Engineering degree in aircraft manufacturing engineering from Shenyang Aerospace University, in July 2003.

He has led and participated in several major projects. In one such project, he independently developed a flexible control system for light aircraft and carried out its modular design. He holds 18 patents and has published more than ten academic papers. His main research directions include the design of electric flight control systems; and the research and design of multirotor UAVs, unmanned helicopters, lightweight autogyros (two-person), lightweight electric helicopters (single-person), and unmanned electric helicopters.

Mr. Wang has received several accolades, including the first prize of the China Society of Aeronautics and Astronautics Science and Technology Award, in 2017. He has been honored twice as an Outstanding Scientific and Technological Worker in his city.

LEI PEI was born in Liaoning, China, in 1997. She received the B.S. degree in automation from the City Institute, Dalian University of Technology, Dalian, China, in 2020. She is currently pursuing the M.S. degree in electronic information with Shenyang Aerospace University, Shenyang, China.

She holds one patent and one EI conference paper. Her research interests include helicopter attitude control and measurement and machine control technology.

ZHENG-MING CHA was born in 1979.

He is currently with AVIC Changhe Aircraft Industry (Group) Company Ltd., as a Senior Engineer. He has been engaged in helicopter research and production for more than 20 years, and successively engaged in helicopter technology and equipment manufacturing, helicopter operation and maintenance management. He is responsible for international subcontracting and the organization of research and production of multiple types of helicopters. He has a wealth of experience in helicopter research and production.